Available online at www.sciencedirect.com
SCIENCE DIRECT®
Journal of Solid State Chemistry 177 (2004) 1717–1722
JOURNAL OF SOLID STATE CHEMISTRY
http://elsevier.com/locate/jssc

Hydrothermal synthesis, structure, and catalytic properties of $UO_2Sb_2O_4$

Richard E. Sykora, Joseph E. King, Andreas J. Illies, and Thomas E. Albrecht-Schmitt*

Department of Chemistry, Auburn University, 179 Chemistry Building, Auburn, AL 36849, USA

Received 2 October 2003; received in revised form 13 December 2003; accepted 30 December 2003

Abstract

A new uranyl antimonite, $UO_2Sb_2O_4$ (**1**), has been prepared from the hydrothermal reaction of UO_3 with Sb_2O_3 and KCl. The structure of **1** consists of neutral two-dimensional $^2_\infty[UO_2Sb_2O_4]$ layers. The U(VI) centers are ligated by two *trans* oxo ligands and four square pyramidal antimonite anions. In addition, the U(VI) also forms long contacts with two additional oxygen atoms that are distorted by 12.7(2)° out of the equatorial plane perpendicular to the uranyl unit. These long interactions are significant owing to evidence supplied by bond valence sum calculations. The two-dimensional layers found in **1** are built from one-dimensional chains formed from edge-sharing UO_6 octahedra that run along the *b*-axis, and are linked together by $[Sb_2O_4]^{2-}$ chains. A flow microreactor system has been used to study the catalytic activity of **1**, and these results show that it can be used as a catalyst in the conversion of propene and O_2 to acrolein. Crystallographic data: **1**, monoclinic, space group $C2/m$, $a = 13.490(2)$ Å, $b = 4.0034(6)$ Å, $c = 5.1419(8)$ Å, $\beta = 104.165(3)°$, $Z = 2$, Mo$K\alpha$, $\lambda = 0.71073$, $R(F) = 1.74\%$ for 30 parameters with 365 reflections with $I > 2\sigma(I)$.

Keywords: Hydrothermal; Uranyl; Oxoanion; Catalysis

1. Introduction

Uranium-based catalysts have been utilized in the total oxidation of organic chlorocarbons to CO_2 and HCl [1], the conversion of NO to N_2 and O_2 [2], the oxidative demethylation of toluene [3], and the ammoxidation of *d*-limonene to trimethylpyridine [4]. Other catalytic processes, whereby propene is converted to acrolein or acrylonitrile through the use of uranium antimony oxides, have been studied extensively [5–11], especially by The Standard Oil Company (Ohio) where these compounds were used as catalysts [12–14] to carry out the ammoxidation of propene [6]. The proposed mechanism for the oxidation or ammoxidation of propene to acrolein or acrylonitrile, respectively, involves a π-allylic intermediate where U(V) and Sb(V) are both present [5]. Oxygen transfer to the alkene has been probed by using $^{18}O_2$-enriched gas, and a time delay in the production of ^{18}O-enriched acrolein provides evidence that interstitial oxygen is active in the oxidation process, and gaseous oxygen replaces the oxygen lost from the crystalline lattice [8]. There are two main crystalline U/Sb/O phases, $USbO_5$ and USb_3O_{10}, that have been structurally characterized by powder X-ray diffraction [6,15], as well as by other spectroscopic and physical property measurements [5,16–18], but single-crystal structures have not been determined for either material. In general, the phases are poorly defined because most syntheses lead to product mixtures that hinder characterization, and in fact most catalysts that are used contain a mixture of both oxides. $USbO_5$ and USb_3O_{10} have both been shown to be highly active for oxidative catalysis, although the latter is more selective for acrylonitrile production [5].

Of major importance in the production of new catalytic materials is the incorporation of redox-active centers that allow for electron transfer. Therefore, to effectively design a new catalyst it is desirable to understand the structural features as well as the composition of the catalyst, because the oxidation state of many elements strongly influences their coordination environments. This is true for uranium as well as antimony. Uranium(VI) is stabilized by the formation of

*Corresponding author. Fax: +334-844-6959.
E-mail address: alberth@auburn.edu (T.E. Albrecht-Schmitt).

0022-4596/$ - see front matter © 2004 Elsevier Inc. All rights reserved.
doi:10.1016/j.jssc.2003.12.033

the predominantly linear uranyl, UO_2^{2+}, cation, although oxidation states lower than uranium(V) do not contain this moiety. This cation is typically bound by four, five, or six ligands perpendicular to the uranyl axis yielding tetragonal, pentagonal, and hexagonal bipyramids. For Sb(V), the coordination environment in oxides is generally octahedral [19–21], while Sb(III) contains a stereochemically active lone pair of electrons, and thus forms lower symmetry trigonal pyramidal [22] or square pyramidal [19,23] coordination environments. The structures and even the compositions [6,15] reported for $USbO_5$ and USb_3O_{10} have been contradictory and this is a major downfall in fully understanding the catalytic cycle of these catalysts.

Using hydrothermal synthesis, our group has recently prepared and structurally characterized a number of uranium/main-group oxides in the form of uranyl iodates [24–27], periodates [28,29], selenites [30,31], and tellurites [32,33] such as: $UO_2(IO_3)_2$ [24], $UO_2(IO_3)_2(H_2O)$ [24], $K_2[(UO_2)_2(VO)_2(IO_6)_2O]\cdot H_2O$ [28], $Pb[UO_2(SeO_3)_2]$ [30], and $Na_8[(UO_2)_6(TeO_3)_{10}]$ [32]. We have also extended these studies to include the preparation of uranium/antimony oxides using hydrothermal reactions. Herein, we report the single-crystal structure of the first hydrothermally produced uranyl antimonite, $UO_2Sb_2O_4$ (**1**), and preliminary results on its catalytic properties.

2. Experimental

2.1. Syntheses

UO_3 (99.8%, Alfa-Aesar), Sb_2O_3 (99.6%, Alfa-Aesar), and KCl (Ultrapure, Alfa-Aesar) were used as received. Distilled and millipore filtered water with a resistance of 18.2 MΩ was used in all reactions. Reactions were run in Parr 4749 23-mL autoclaves with PTFE liners. The reaction reported produced the highest yield of the desired compound. SEM/EDX analyses were performed using a JEOL 840/Link Isis instrument. U and Sb percentages were calibrated against standards. Typical results are within 3% of actual ratios. IR spectra were collected on a Nicolet 5PC FT–IR spectrometer from KBr pellets. *Warning: While the UO_3 contains depleted U, standard precautions for handling radioactive materials should be followed. Old sources of depleted U should not be used, as the daughter elements of natural decay are highly radioactive and present serious health risks.*

2.2. $UO_2Sb_2O_4$ (1)

UO_3 (787 mg, 2.75 mmol), Sb_2O_3 (802 mg, 2.75 mmol), and KCl (410 mg, 5.50 mmol) were loaded in a 23-mL PTFE-lined autoclave. Water (4 mL) was then added to the solids. The autoclave was sealed and placed in a box furnace and then heated to 180°C where the reaction occurred under autogenously generated pressure. After 89 h the furnace was cooled at 9°C/h to 23°C. The product mixture included clusters of orange crystals of **1** and a fine yellow powder immersed in a pale yellow mother liquor. The mother liquor was decanted from the products, which was then washed with water followed by methanol and allowed to dry. The orange crystals of **1** could manually be separated from the yellow powder to afford a yield of 439 mg (28% based on U). EDX analysis for $UO_2Sb_2O_4$ provided a U:Sb ratio of 1:2. IR (KBr, cm^{-1}): 850 (υ_{UO}, s), 638 (υ_{SbO}, s), 509 (s).

2.3. Crystallographic studies

A single crystal of **1** with approximate dimensions of $0.050 \times 0.038 \times 0.010\,mm^3$ was selected and mounted on a glass fiber. The crystal was then aligned on a Bruker SMART APEX CCD diffractometer and cooled to −80°C with an Oxford Cryostat. For the crystal of **1**, intensity measurements were performed using graphite monochromatic Mo$K\alpha$ radiation from a sealed tube and a monocapillary collimator. SMART was used for preliminary determination of the cell constants and data collection control. The intensities of reflections of a sphere were collected by a combination of three sets of exposures (frames). Each set had a different φ angle for the crystal and each exposure covered a range of 0.3° in ω. A total of 1800 frames were collected with an exposure time per frame of 60 s.

For **1**, determination of integral intensities and global cell refinement were performed with the Bruker SAINT (v 6.02) software package using a narrow-frame integration algorithm. A face-indexed analytical absorption correction was initially applied using XPREP [34]. Individual shells of unmerged data were corrected analytically and exported in the same format. These files were subsequently treated with a semi-empirical absorption correction by SADABS [35,36]. The program suite SHELXTL (v 5.1) was used for space group determination (XPREP), direct methods structure solution (XS), and least-squares refinement (XL) [34]. The systematic absences were consistent with a C-centered cell, narrowing the possible space groups to *Cm*, *C*2, and *C*2/*m*. The structure was initially solved and refined in the noncentrosymmetric space group *C*2. After further inspection, the space group assignment *C*2/*m* was made. The final refinements included anisotropic displacement parameters for all atoms and a secondary extinction parameter. Some crystallographic details are listed in Table 1 and the final positional parameters for **1** can be found in Table 2. Tables of anisotropic displacement parameters for **1** are available in the supporting CIF file.

Table 1
Crystallographic data for $UO_2Sb_2O_4$ (**1**)

Formula	$UO_2Sb_2O_4$
Formula mass	577.53
Color and habit	Orange, tablet
Space group	$C2/m$
a (Å)	13.490(2)
b (Å)	4.0034(6)
c (Å)	5.1419(8)
β (deg)	104.165(3)
V (Å^3)	269.24(7)
Z	2
T (°C)	−80
λ (Å)	0.71073
Maximum 2θ (deg)	56.58
ρ_{calcd} (g/cm^3)	7.124
μ(Mo$K\alpha$) (cm^{-1})	399.16
$R(F)$ for $F_o^2 > 2\sigma(F_o^2)$[a]	0.0174
$R_w(F_o^2)$[b]	0.0413

[a] $R(F) = \sum||F_o| - |F_c||/\sum|F_o|$.
[b] $R_w(F_o^2) = [\sum[w(F_o^2 - F_c^2)^2]/\sum wF_o^4]^{1/2}$.

Table 2
Atomic coordinates and equivalent isotropic displacement parameters for $UO_2Sb_2O_4$ (**1**)

Atom	x	y	z	U_{eq} (Å^2)[a]
U(1)	1/2	0	1/2	0.008(1)
Sb(1)	0.30844(3)	−1/2	0.75725(9)	0.007(1)
O(1)	0.4309(4)	−1/2	0.620(1)	0.009(1)
O(2)	0.1963(4)	−1/2	0.401(1)	0.009(1)
O(3)	0.4171(4)	0	0.166(1)	0.014(1)

[a] U_{eq} is defined as one-third of the trace of the orthogonalized $\mathbf{U}_{ij}$ tensor.

2.4. Catalytic tests

A flow microreactor was used to study the catalytic activity of $UO_2Sb_2O_4$ (**1**). Propene (99.1%, Conley), oxygen (5.0, BOC), and helium (6.0, Matheson) were used as received. The reaction chamber was built from two 12 in lengths of 1/4 in o.d. stainless steel tubing that were connected by a stainless steel swagelock fitting to allow for sample loading. A tube furnace was employed to hold the temperature of the reaction chamber at 400°C. A U-tube glass bubbler was attached to the back of the apparatus to trap reaction products. Two septa ports were included to allow for in-stream analysis as well as analysis of the MeOH solvent used in the bubbler.

The feed gases were metered by flow control devices and premixed prior to being introduced into the reaction chamber. The rate of flow was 30 mL/min for propene, 60 mL/min for O_2, and 60 mL/min for He. The gases were passed across approximately 70 mg of **1**. In-stream samples as well as bubbler solutions were analyzed on a TRIOS GC/MS system using an AT-624 6 m × 0.25 mm ID × 1.4 μm column programmed between 35°C and 220°C. Resultant peaks in the chromatogram were analyzed by the use of standards as well as mass spectra. Blank runs carried out at 400°C were used to determine that there were negligible reactions on the walls of the reactor.

3. Results and discussion

3.1. Syntheses

The hydrothermal reaction of UO_3, Sb_2O_3, and KCl has led to the production of a new uranyl antimonite, $UO_2Sb_2O_4$ (**1**). While neither K^+ nor Cl^- ions are incorporated into the structure of **1**, as determined from semi-quantitative EDX measurements, direct reactions of UO_3 and Sb_2O_3 under similar reaction conditions have not been successful in producing **1**. In addition, CsCl has been used in place of KCl to successfully produce **1**. We speculate that the role of KCl is as a source of Cl^-, a known mineralizer agent, that aids in solubilizing the UO_3 and in recrystallizing **1** [37,38]. Compound **1** has only been produced along with a fine yellow powder. Elemental analysis indicates that the powder contains U, Sb, and O. However, powder X-ray diffraction experiments reveal that this solid is largely amorphous. Despite carrying out a number of reactions with varying reactant stoichiometries, temperatures (up to 425°C in gold ampules), and solvent fill levels, **1** has not been produced in pure form.

3.2. Structure of $UO_2Sb_2O_4$ (**1**)

The structure of **1** contains two-dimensional sheets as do the majority of U(VI) structures [39]. A nominal UO_6 subunit forms the backbone of the structure, although there is strong evidence that the coordination environment around uranium would be better described as a UO_8 distorted hexagonal bipyramid. The structural building unit for **1** is shown in Fig. 1. In addition to the two terminal oxo groups, the U(1) coordination environment is completed by four bridging O(1) and two bridging O(2) atoms, both from antimonite anions. The bridging O(1) atoms are perpendicular to the uranyl unit as expected for U(VI) compounds; however, the two O(2) atoms deviate from the orthogonal plane by 12.7(2)° (Fig. 1). The U(1)–O(2) interactions are 2.815(5) Å, 0.4–0.6 Å longer than expected for a U–O equatorial bond length [24–33], while the U(1)–O(1) bond lengths of 2.354(3) Å are well within the expected range [24–33]. By evaluating the bond angles of the equatorial O(1) atoms, an argument can be made that the O(2) atoms are indeed making a significant bonding contribution. The O(1)–U(1)–O(1)′ angle is highly compressed at 63.5(2)° and the O(1)′–U(1)–O(1)″ angle

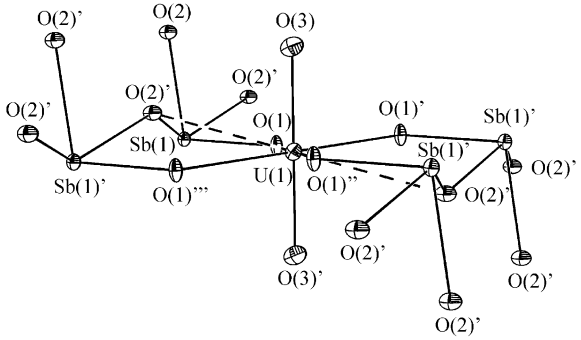

Fig. 1. A view of the local environment of uranium in $UO_2Sb_2O_4$ (**1**) showing the highly distorted hexagonal bipyramidal environment with two long U(1)–O(2) interactions with a distance of 2.815(5) Å. 50% displacement ellipsoids are depicted.

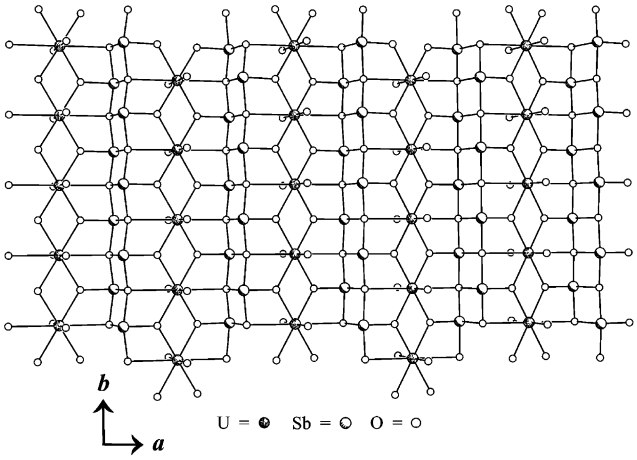

Fig. 2. An illustration of the UO_8 distorted hexagonal bipyramidal units in $UO_2Sb_2O_4$ (**1**) that edge share along the *b*-axis to form uranium oxygen chains that are further linked into two-dimensional $^{2}_{\infty}[UO_2Sb_2O_4]$ layers by the bridging $^{1}_{\infty}[Sb_2O_4]^{2-}$ chains.

is correspondingly expanded with a value of 116.5(2)° in order to compensate for the O(2) atoms. Also, we have conducted bond valence sum calculations including just the six closest neighbor O(1) and O(3) atoms, and also with all eight interacting oxygen atoms and have found values of 5.66 and 5.79, respectively, which show that the O(2) atoms form significant bonding interactions [40,41]. For further purposes of discussion, therefore, we will refer to the uranium coordination as a distorted hexagonal bipyramid.

The UO_8 distorted hexagonal bipyramidal units edge share along the *b*-axis to form uranium oxygen chains that are further linked into two-dimensional $^{2}_{\infty}[UO_2Sb_2O_4]$ layers by the bridging $^{1}_{\infty}[Sb_2O_4]^{2-}$ chains as shown in Fig. 2. A small interlayer spacing of 4.986 Å leads to a density of 7.124 g/cm^3 and is higher than found for most other uranium/main-group oxides [24,30] that have been produced from hydrothermal syntheses. A view along the crystallographic *b*-axis showing the stacking of the layers in **1** is shown in

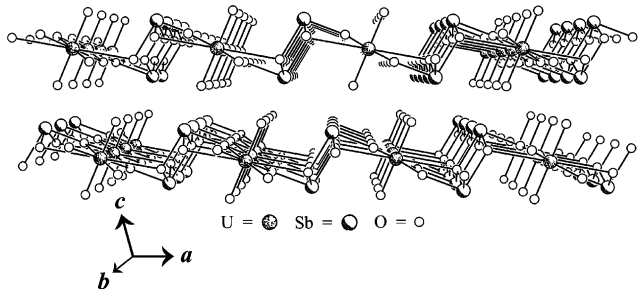

Fig. 3. A view along the crystallographic *b*-axis showing the stacking of the layers in $UO_2Sb_2O_4$ (**1**).

Table 3
Selected bond distances and interactions (Å) and angles (deg) for $UO_2Sb_2O_4$ (**1**)

Distances (Å)			
U(1)–O(1) × 4	2.354(3)	Sb(1)–O(1)	1.948(5)
U(1)–O(2) × 2	2.815(5)	Sb(1)–O(2)	2.070(5)
U(1)–O(3) × 2	1.805(5)	Sb(1)–O(2) × 2	2.156(2)
Angles (deg)			
O(1)–U(1)–O(1)′	63.5(2)	O(1)–Sb(1)–O(2)	100.4(2)
O(1)′–U(1)–O(1)″	116.5(2)	O(1)–Sb(1)–O(2)′	79.18(14)
O(3)–U(1)–O(3)′	180	O(2)–Sb(1)–O(2)′	73.63(13)
		O(2)′–Sb(1)–O(2)″	136.3(3)

Fig. 3. The lone pairs on the antimony atoms point toward adjacent layers and form long interactions of 3.011 Å between the antimony atoms of one layer and the O(3) atoms of neighboring layers that help hold the structure together.

The $^{1}_{\infty}[Sb_2O_4]^{2-}$ chains found in $UO_2Sb_2O_4$ are comprised of four coordinate SbO_4 square pyramids, containing a lone pair, that edge share along the *b*-axis and are similar to Sb–O chains found in $SbNbO_4$ and $SbTaO_4$ [42,43]. All of the oxygen atoms bound to Sb(1) are at least μ_3 and if the 2.815(5) Å U(1)···O(2) interactions are considered bonds, then three of the antimonite oxygens are μ_4. As expected, the shortest Sb–O bond length of 1.948(5) Å is to the truly μ_3 O(1). The bond valence sum calculated for Sb(1) [41] is 3.06 and is consistent with Sb(III). Additional bond lengths and angles for **1** can be found in Table 3.

3.3. Catalytic results

We have begun testing of uranyl iodates, selenites, tellurites, and antimonites as catalysts for the selective oxidation of propene to produce acrolein as has been done with previously known uranium antimony oxides [5–14]. We have compared the results that we have obtained from these measurements with known selective oxidation catalysts and standards for observed products. When propene, oxygen, and helium are passed over $UO_2Sb_2O_4$ (**1**) in a microreactor at 400°C trace amounts of acrolein were observed to form via GC/MS

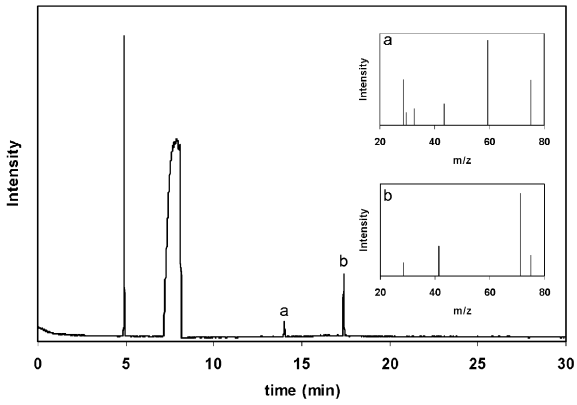

Fig. 4. A gas chromatogram of propene (4.89 min.), methanol (7.88 min.), (a) 1,1-dimethoxyethane (14.01 min), and (b) dimethyl acetal acrolein (17.38 min) with mass spectra inset of the last two compounds.

measurements. The catalyst is quite robust and remains active at 400°C for more than 4 h. The efficiency of **1**, which we estimate to be less than 1%, for this process is only a small fraction of that produced when compared to the industrially relevant bismuth molybdate, Bi_2MoO_6. However, we noted that when gaseous methanol was added to the stream by bubbling the reactant gases through a bubbling tube that both 1,1-dimethoxyethane (14.01 min) and dimethyl acetal acrolein (17.38 min) could be formed, as shown in Fig. 4. While the molecular ion peaks for both compounds are absent, they can be identified from their fragmentation patterns [44]. The formation of dimethyl acetal acrolein apparently involves nucleophilic attack on the bound allyl group by methanol, which is a new reaction for uranium catalysts. We speculate that the 1,1-dimethoxyethane forms from the same attack of the allyl group by methanol followed by the loss of the methane, which would not be detected using our experimental set-up. Further work needs to be carried out in order to fully understand the mechanism and kinetics of these reactions.

3.4. Auxiliary material

Further details of the crystal structure investigation may be obtained from the Fachinformationzentrum Karlsruhe, D-76344 Eggenstein-Leopoldshafen, Germany (Fax: (+49)7247-808-666; E-mail: crysdata@fiz-karlsruhe.de) on quoting depository numbers CSD 413442.

Acknowledgments

This research was sponsored by the US Department of Energy, Heavy Elements Program, Grant No. DE-FG02-01ER15187.

References

[1] G.J. Hutchings, C.S. Heneghan, I.D. Hudson, S.H. Taylor, Nature 384 (1996) 341.
[2] S.D. Pollington, A.F. Lee, T.L. Overton, P.J. Sears, P.B. Wells, S.E. Hawley, I.D. Hudson, D.F. Lee, V. Ruddock, Chem. Commun. 8 (1999) 725.
[3] J.G. Steenhof De Jong, C.H.E. Guffens, H.S. Van Der Baan, J. Catal. 26 (1972) 401.
[4] S.R. Dolhyj, L.J. Velenyi, Ind. Eng. Chem. Prod. Res. Dev. 19 (1980) 194.
[5] R.K. Grasselli, D.D. Suresh, J. Catal. 25 (1972) 273.
[6] R.K. Grasselli, J.L. Callahan, J. Catal. 14 (1969) 93.
[7] H. Collette, V. Deremince-Mathieu, Z. Gabelica, J.B. Nagy, E.G. Derouane, J.J. Verbist, J. Chem. Soc. Faraday Trans. 2 83 (1987) 1263.
[8] P. Pendleton, D. Taylor, J. Chem. Soc. Faraday Trans. 1 72 (1976) 1114.
[9] L.D. Krenzke, G.W. Keulks, A.V. Sklyarov, A.A. Firsova, M.Y. Kutirev, L.Y. Margolis, O.V. Kyrlov, J. Catal. 52 (1978) 418.
[10] E.V. Hoefs, J.R. Monnier, G.W. Keulks, J. Catal. 57 (1979) 331.
[11] H. Baussart, R. Delobel, M. LeBras, D. LeMaguer, J.-M. Leroy, J. Chem. Soc. Faraday Trans. 1 78 (1982) 485.
[12] J.L. Callahan, W.R. Knipple, US Patent 3,341,471, September 12, 1967 (to The Standard Oil Company (Ohio)).
[13] J.L. Callahan, B. Gertisser, US Patent 3,198,750, August 3, 1965 (to The Standard Oil Company (Ohio)).
[14] J.L. Callahan, B. Gertisser, US Patent 3,308,151, March 7, 1967 (to The Standard Oil Company (Ohio)).
[15] R.K. Grasselli, D.D. Suresh, K. Knox, J. Catal. 18 (1970) 356.
[16] S.E. Golunski, T.G. Nevell, D.J. Hucknall, J. Chem. Soc. Faraday Trans. 1 81 (1985) 1121.
[17] S.E. Golunski, T.G. Nevell, D.J. Hucknall, J. Catal. 88 (1984) 448.
[18] T. Birchall, A. Sleight, J. Catal. 53 (1978) 280.
[19] K.M. Ok, N.S.P. Bhuvanesh, P.S. Halasyamani, J. Solid State Chem. 161 (2001) 57.
[20] P. Koehl, D. Reinen, Z. Anorg. Allg. Chem. 433 (1977) 81.
[21] S.A. Ivanov, V.E. Zavodnik, Kristallografiya 35 (1990) 842.
[22] A. Laarif, F.R. Theobald, H. Vivier, A.W. Hewat, Z. Kristallogr. 167 (1984) 117.
[23] V.I. Ponomarev, O.S. Filipenko, L.O. Atovmyan, N.V. Rannev, S.A. Ivanov, Y.N. Venevtsev, Kristallografiya 26 (1981) 341.
[24] A.C. Bean, S.M. Peper, T.E. Albrecht-Schmitt, Chem. Mater. 13 (2001) 1266.
[25] A.C. Bean, C.F. Campana, O. Kwon, T.E. Albrecht-Schmitt, J. Am. Chem. Soc. 123 (2001) 8806.
[26] A.C. Bean, T.E. Albrecht-Schmitt, J. Solid State Chem. 161 (2001) 416.
[27] R.E. Sykora, A.C. Bean, B.L. Scott, W. Runde, T.E. Albrecht-Schmitt, J. Solid State Chem., 2004, in press.
[28] R.E. Sykora, T.E. Albrecht-Schmitt, Inorg. Chem. 42 (2003) 2179.
[29] T.A. Sullens, T.E. Albrecht-Schmitt, Unpublished results.
[30] P.M. Almond, T.E. Albrecht-Schmitt, Inorg. Chem. 41 (2002) 1177.
[31] P.M. Almond, S.M. Peper, E. Bakker, T.E. Albrecht-Schmitt, J. Solid State Chem. 168 (2002) 358.
[32] P.M. Almond, M.L. McKee, T.E. Albrecht-Schmitt, Angew. Chem. Int. Ed. 41 (2002) 3426.
[33] P.M. Almond, T.E. Albrecht-Schmitt, Inorg. Chem. 41 (2002) 5495.
[34] G.M. Sheldrick, SHELXTL PC, Version 5.0, An Integrated System for Solving, Refining, and Displaying Crystal Structures from Diffraction Data, Siemens Analytical X-ray Instruments, Madison, WI, 1994.

[35] SADABS, Program for absorption correction using SMART CCD based on the method of Blessing: R.H. Blessing, Acta Crystallogr. A51 (1995) 33.
[36] F.Q. Huang, J.A. Ibers, Inorg. Chem. 40 (2001) 2602.
[37] R.E. Sykora, P.M. Almond, T.E. Albrecht-Schmitt, Inorg. Chem. 42 (2003) 3788.
[38] A.C. Bean, M. Ruf, T.E. Albrecht-Schmitt, Inorg. Chem. 40 (2001) 3959.
[39] P.C. Burns, M.L. Miller, R.C. Ewing, Can. Miner. 34 (1996) 845.
[40] P.C. Burns, R.C. Ewing, F.C. Hawthorne, Can. Miner. 35 (1997) 1551.
[41] N.E. Brese, M. O' Keeffe, Acta Crystallogr. B 47 (1991) 192.
[42] V.I. Ponomarev, O.S. Filipenko, L.O. Atomyan, N.V. Rannev, S.A. Ivanov, Yu.N. Venevtsev, Kristallografiya 26 (1981) 341.
[43] K. Dihlstroem, Z. Anorg. Allg. Chem. 239 (1938) 57.
[44] http://webbook.nist.gov/chemistry.